Absorption, photoluminescence, and resonant Rayleigh scattering probes of condensed microcavity polaritons

F. M. Marchetti,[1,*] J. Keeling,[2,†] M. H. Szymańska,[3] and P. B. Littlewood[1]
[1]*Cavendish Laboratory, University of Cambridge, Madingley Road, Cambridge CB3 0HE, United Kingdom*
[2]*Department of Physics, Massachusetts Institute of Technology, 77 Massachusetts Avenue, Cambridge, Massachusetts 02139, USA*
[3]*Clarendon Laboratory, Department of Physics, University of Oxford, Parks Road, Oxford OX1 3PU, United Kingdom*
(Received 3 August 2006; published 20 September 2007)

We investigate and compare different optical probes of a condensed state of microcavity polaritons in expected experimental conditions of nonresonant pumping. We show that the energy- and momentum-resolved resonant Rayleigh signal provides a distinctive probe of condensation as compared to, e.g., photoluminescence emission. In particular, the presence of a collective sound mode both above and below the chemical potential can be observed, as well as features directly related to the density of states of particle-hole-like excitations. Both resonant Rayleigh response and the absorption and photoluminescence are affected by the presence of quantum well disorder, which introduces a distribution of oscillator strengths between quantum well excitons at a given energy and cavity photons at a given momentum. As we show, this distribution makes it important that in the condensed regime, scattering by disorder is taken into account to all orders. We show that, in the low-density linear limit, this approach correctly describes inhomogeneous broadening of polaritons. In addition, in this limit, we extract a linear blueshift of the lower polariton versus density, with a coefficient determined by temperature and by a characteristic disorder length.

DOI: 10.1103/PhysRevB.76.115326 PACS number(s): 78.35.+c, 71.36.+c, 78.40.Pg, 71.45.−d

I. INTRODUCTION

Since the prediction of Keldysh and Kopaev,[1] there has been a long and intense pursuit to realize a condensed phase in solid state excitonic, and related, systems. In particular, polaritons in semiconductor microcavities, the coupled eigenstates of an exciton with a cavity photon,[2,3] represent ideal candidates for observing condensation phenomena. The very light mass of these composite bosonic particles promises relatively high transition temperatures. In the past decade, improvements in the growth technology of semiconductor heterostructures have made the study of high-quality strongly coupled planar microcavities almost routine for III-V and II-VI semiconductors. The high degree of external control of these systems and the possibility of their direct detection have opened the route toward a new generation of fast optical matter-wave lasers and amplifiers.[4–8] More recently, concerted experimental efforts have been devoted to the realization of a Bose-Einstein condensate of microcavity polaritons.[4,9–14]

On the experimental side, a challenge to the realization of a condensed polariton phase might be represented by the finite quality of the cavity mirrors and the resultant short polariton lifetime, of the order of picoseconds. In addition, due to the "bottleneck effect,"[15] the relaxation of polaritons to the zero momentum state can be delayed, hindering the creation of a thermal population in the lowest energy state. It has, however, been recently shown[13,14,16] that thermalization processes due to particle-particle scattering can be dramatically magnified by increasing the value of the (nonresonant) pump power and by positively detuning the cavity energy above the excitonic energy. Under these conditions, the progress toward a zero momentum quasiequilibrium condensate has been significant,[4,5,9–13] including a nonlinear threshold behavior in the emission intensity at zero momentum,[4,5,9,13] the investigation of the second order coherence function,[9] a characteristic change in the momentum space distribution above threshold,[10,13] and evidence that the equilibration time is shorter than the polariton lifetime has been seen.[13] Finally, very recently, a clear demonstration of condensation of cavity polaritons has been achieved in CdTe.[14] Kasprzak *et al.* have shown that condensation of equilibrated polaritons can be achieved for effective temperatures around 20 K, and evidence for condensation has been seen in the occupation function, in the first order coherence (both in time and in space), and in the spontaneous appearance of linear polarization of the condensate emission.

Alongside the experimental effort, a significant theoretical effort has been invested in analyzing properties and predicting signatures of polariton condensation.[17–29] Much of this work focuses on modeling the conditions under which condensation can occur, both in equilibrium,[17,20–22] and considering the effects of pumping and decay.[23,26,28,29] Possible signatures include the nonlinear relation of emission at zero momentum to pumping power,[27–29] changes to the linewidth,[26,27,29] the photoluminescence (PL) spectrum and the angular distribution of radiation,[21,22] and spontaneous polarization of emitted radiation.[24]

In this paper, we discuss the optical properties of condensed polaritons, focusing our interests on absorption, PL, and resonant Rayleigh scattering (RRS). From our study, we conclude that RRS, the coherent scattering by disorder of polaritons into directions other than that of the original probe, represents a powerful tool for investigating the condensed phase. We will show that signatures of condensation are visible in the RRS spectrum, allowing a direct probe of the collective excitation properties of the polariton condensate. In particular, we will show that, above the threshold for condensation, strong emission from the collective sound mode both above and below the chemical potential can be

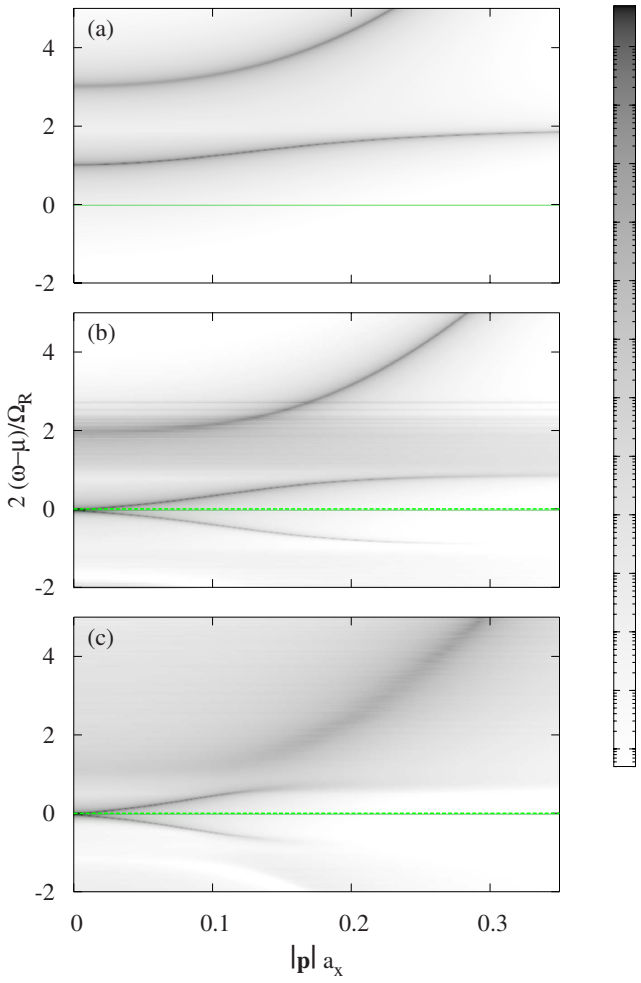

FIG. 1. (Color online) Contour plot of the disorder averaged RRS intensity $\langle I_{\mathbf{pq}}(\omega)\rangle$ for $|\mathbf{p}|=|\mathbf{q}|$ as a function of the dimensionless momentum $|\mathbf{p}|a_x$ and rescaled energy $2(\omega-\mu)/\Omega_R$, for zero detuning, Rabi splitting $\Omega_R=26$ meV, temperature $k_BT=20$ K, and a disorder strength characterize by an inverse scattering time $1/\tau=1.16$ meV: (a) noncondensed regime (dimensionless density $\rho\simeq 0$), (b) condensed regime ($\rho\simeq 7.8\times 10^{-3}$), and (c) condensed regime ($\rho\simeq 6.7\times 10^{-2}$). (The parameters chosen for these plots are the same as those used later for spectral weight and photoluminescence.) The value of the chemical potential is explicitly marked [horizontal green (gray) line]. While in the noncondensed regime, RRS emission is always above the chemical potential, in the condensed phase, emission from the collective sound mode is seen both above and below the chemical potential.

seen in the RRS spectra (see Fig. 1). In contrast, such features are expected to be much harder to observe in usual PL emission spectra, where the spectrum is dominated by the very strong condensate emission at the chemical potential, which is likely to mask these more subtle features. In addition, we will show that the RRS spectra directly reflects the disorder averaged density of states of excitonic particle-hole-like excitations, i.e., bound excitons coupled to the coherent photon field.

Resonant Rayleigh scattering depends on disorder to scatter polaritons between momentum states. In order to carry on our analysis, we introduce a realistic description of disorder and analyze its effects on RRS and, more generally, on other optical probes, such as absorption and PL. To do this, we make use of a quantitatively accurate model for exciton disorder[30–32] and numerically evaluate the distribution of excitonic energies and oscillator strengths associated with a given disorder potential. An accurate treatment of exciton disorder for quantum wells in microcavities is important because the large ratio of exciton mass to photon mass means that those exciton states with the most contribution to the thermally populated polaritons are strongly localized, i.e., cannot be treated within the first Born approximation. Such a treatment shows that, for a given exciton energy and momentum, there is still a distribution of possible oscillator strengths. For the exciton states relevant to polariton formation, the distribution of oscillator strengths varies from a narrow Gaussian at low energies (below the band edge) to a Porter-Thomas distribution at high energies, as is known from previous works.[30–32] Here, we study the effect of this distribution on the many-body physics and, in particular, on RRS and PL spectra.

In this paper, we consider the case relevant to the existing CdTe or GaAs microcavities of high-quality quantum wells, where the typical excitonic disorder amplitude is smaller than the Rabi splitting. In this regime, we can make use of the *coupled oscillator model* or wave vector conserving approximation, as explained in Ref. 33. As will be explained in more detail later on, this corresponds to approximating the full exciton Green's function by its momentum-diagonal part (or, equivalently, considering its disorder average) and treating perturbatively the off-diagonal terms. In this way, the translational invariance broken by the presence of the disorder is restored, polaritons have a defined wave vector, and, at high enough densities, polaritons condense in the lowest momentum state. Such a treatment implies that excitonic disorder, being on short length scales, does not lead to spatial inhomogeneity on the length scale associated with the polariton. Extended polaritons are formed from a superposition of many localized excitons, therefore recovering translational invariance at the level of polaritons. At low densities, in the noncondensed state, many observable properties can be adequately described by the coupled oscillator model and so can be found from the mean squared oscillator strength at a given energy. In this limit, our method recovers the well known results for the inhomogeneous broadening of the polariton PL[33,34] and—by considering in addition the mean fourth power of the oscillator strength—the averaged RRS response.[35–38] However, when condensed, there are observable effects associated with the full distribution of oscillator strengths. In particular, the nonvanishing probability of excitons to have arbitrarily small oscillator strengths has direct consequences for optical probes, including both RRS and PL.

In Ref. 25, we considered specific aspects of resonant Rayleigh scattering arising from the model discussed in this paper. Here, we provide and compare further experimental probes of condensation, and discuss the underlying physical mechanisms involved. All these optical probes, including RRS, are in addition to a nonresonant pumping of the microcavity polaritons. A related problem is studied in Ref. 39. There, the Rayleigh scattering of a strong resonant pump is

considered (treating disorder perturbatively), thus the probe is the pump. In this paper, in contrast, one has to distinguish two types of coherence. The first type is the internal coherence of the condensed system, which arises spontaneously following nonresonant pumping. The second type is the coherent scattering of an external laser probe on disorder, which can be strongly modified by the presence of the condensate.

The form of the density of states, optical density, and distribution of oscillator strengths found from the numerical calculations is also important in other thermodynamic properties and probes of polaritons. One such example is the calculation of the linear blueshift vs density in the low-density regime. The inclusion of exciton states that couple weakly to photons extends the validity of the current model to densities beyond those in similar treatments[17,21] and provides a stronger basis for the use of those models in the regimes where they are valid.

The paper is arranged in the following sections: We introduce our model of the system in Sec. II, which makes use of numerically evaluated energies and wave functions of excitons in a disordered quantum well, as evaluated in Sec. II B. Section III describes the optical probes such as spectral weight and photoluminescence (Sec. III A) and resonant Rayleigh scattering (Sec. III C). Conclusions are collected in Sec. IV, while the Appendix explains how one can detect RRS using phase sensitive measurements.

II. MODELING EXCITON POLARITONS IN DISORDERED QUANTUM WELLS

We make use of a model describing localized excitons dipole coupled to a cavity photon mode. This model is discussed in detail elsewhere (see, e.g., Ref. 40 and references therein), so we will only briefly summarize its properties. We will set $\hbar=1$ throughout. The interaction between excitons is approximated by exclusion; i.e., excitons are treated as hard-core bosons. This approximation is accurate as far as the occupancy is restricted to the strongly localized Lifshitz states in the tail below the band edge. All the results described in this paper respect this limit. One can, moreover, show that it is this density regime which is relevant for ongoing experiments in CdTe.[14] Higher energy states, beyond the Lifshitz tail, contribute to the optical response; however, they are only weakly occupied, and so the above limit remains valid.

As described in Ref. 40, these hard-core bosons can be represented by two fermionic states, so that the ground state $|\text{g.s.}\rangle=a_\alpha^\dagger|0\rangle$, and an excitonic state $|\text{ex}\rangle=b_\alpha^\dagger|0\rangle=b_\alpha^\dagger a_\alpha|\text{g.s.}\rangle$. Imposing a constraint on total fermion occupancy, $b_\alpha^\dagger b_\alpha+a_\alpha^\dagger a_\alpha=1$, eliminates the unphysical states $|0\rangle$ and $a_\alpha^\dagger b_\alpha^\dagger|0\rangle$. The effective Hamiltonian is thus

$$\hat{H}=\sum_\alpha \frac{\varepsilon_\alpha}{2}(b_\alpha^\dagger b_\alpha+a_\alpha a_\alpha^\dagger)+\sum_{\mathbf{p}}\omega_{\mathbf{p}}\psi_{\mathbf{p}}^\dagger\psi_{\mathbf{p}}+\frac{1}{\sqrt{L^2}}\sum_\alpha\sum_{\mathbf{p}}(g_{\alpha,\mathbf{p}}\psi_{\mathbf{p}}b_\alpha^\dagger a_\alpha+\text{H.c.}). \quad (1)$$

The exciton energies ϵ_α and transition matrix elements $g_{\alpha,\mathbf{p}}$ are taken from numerical simulations of excitons in a disordered quantum well, as discussed below. It is convenient to rescale this coupling according to

$$g_{\alpha,\mathbf{p}}\mapsto g_{\alpha,\mathbf{p}}\sqrt{\mathcal{R}y_x m_x/2\pi},$$

where $N=\mathcal{R}y_x L^2 m_x/2\pi$ is the inverse level spacing $L^2 m_x/2\pi$, measured in units of the excitonic Rydberg energy. This corresponds to measuring the density of particles per Bohr radius squared. Using these units, we may write the total number of excitations

$$\hat{N}=\sum_\alpha\frac{1}{2}(b_\alpha^\dagger b_\alpha+a_\alpha a_\alpha^\dagger)+\sum_{\mathbf{p}}\psi_{\mathbf{p}}^\dagger\psi_{\mathbf{p}} \quad (2)$$

in a dimensionless form by introducing a dimensionless density of particles $\rho\equiv\langle\hat{N}\rangle/N$, or, equivalently, $\rho=(\langle\hat{N}\rangle/L^2)a_x^2 4\pi\mu/m_x$, where $\langle\hat{N}\rangle/L^2$ is the physical areal density of particles.

What the model Eq. (1) does not include is the Coulomb interaction between excitons with different energies ε_α, i.e., at low densities, on different localization sites $\mathbf{R}_\alpha$. This contribution is expected to be small in the low-density regime. This low-density regime will be observed all the way through this paper. At the same time, we are not including double occupancy of a single exciton energy level, which could be important at higher densities.

A. Exciton states in disordered quantum wells

The problem of an exciton in a disordered quantum well has been studied at some length in the past two decades.[30–32,41–44] Quantum well disorder can arise due to interface and alloy fluctuations and affects the properties of the excitonic linewidth and absorption spectrum. Similar to Refs. 30 and 31, we will assume the external disorder potential to be correlated on a length scale larger than the exciton Bohr radius. Accordingly, we factorize the excitonic in-plane relative and center of mass coordinates

$$\Psi_\alpha(\mathbf{r}_e,\mathbf{r}_h)\simeq\varphi_{1s}(r)\Phi_\alpha(\mathbf{R}),$$

$$\varphi_{1s}(r)=\sqrt{8/\pi a_x^2}e^{-2r/a_x},$$

and assume that the disorder affects only the excitonic center of mass motion $\Phi_\alpha(\mathbf{R})$, while the internal degrees of freedom can be restricted to the ground state hydrogenic state $\varphi_{1s}(r)$. Here, $a_x=\epsilon/e^2\mu_r$ is the exciton Bohr radius and μ_r the reduced mass. Neglecting the transverse degrees of freedom related to the confinement of the excitons in the quantum well, the energy associated with the wave function $\Psi_\alpha(\mathbf{r}_e,\mathbf{r}_h)$ is given by the sum of the relative motion energy E_x [i.e., the band gap minus the exciton binding energy, $\mathcal{R}y_x=(2\mu_r a_x^2)^{-1}=e^4\mu_r/2\epsilon^2$] and the energy related to the center of mass motion ε_α:

$$\left[-\frac{\nabla_{\mathbf{R}}^2}{2m_x}+V(\mathbf{R})+E_x\right]\Phi_\alpha(\mathbf{R})=\varepsilon_\alpha\Phi_\alpha(\mathbf{R}). \quad (3)$$

Here, the effective disorder potential $V(\mathbf{R})$ represents the microscopic structural disorder averaged over the electron-hole

motion.[30] This can be approximated, e.g., with a Gaussian noise correlated on a length scale $\ell_c > a_x$ with variance equal to σ^2:

$$\langle V(\mathbf{R})V(\mathbf{R}')\rangle = (\sigma^2\ell_c^2/L^2)\sum_{\mathbf{q}}^{1/\ell_c} e^{i\mathbf{q}\cdot(\mathbf{R}-\mathbf{R}')},$$

where L^2 is the quantization area. It will be convenient, later on, to introduce the scattering time

$$\tau = \frac{1}{2\pi\nu\sigma^2\ell_c^2},$$

where $\nu = m_x/2\pi$ is the two-dimensional density of states in the clean limit.

In two-dimensional noninteracting systems, all states are localized by the disorder potential. However, the localization length and the character of the excitonic wave function change significantly from below to above the band edge E_x. Well below the band edge, low-energy Lifshitz tail states[45] are well localized in deep potential minima with a nodeless (roughly Gaussian) shape. These states are rare because they occur due to large, rare, fluctuations of the disorder potential. In contrast, higher-energy states above the band edge have a fractal-like shape with many nodes and can be approximated by a random superposition of plane waves with the same momentum $|\mathbf{p}| \simeq \sqrt{2m_x(\varepsilon_\alpha - E_x)}$. Here, the localization mechanism is closely related to quantum mechanical interference effects.

Accordingly, the change of the shape of the center of mass wave functions across the band edge is accompanied by a dramatic change in the excitonic oscillator strength.[31] The oscillator strength describing coupling of a quantum well exciton to light, $g_{\alpha,\mathbf{p}}$, is given by the probability amplitude of finding an electron and a hole at the same position and with the center of mass momentum equal to the photon momentum $\mathbf{p}$, and is, therefore, proportional to the Fourier transform of the center of mass wave function, $\Phi_{\alpha,\mathbf{p}} = \langle \Phi_\alpha | \mathbf{p} \rangle$:

$$g_{\alpha,\mathbf{p}} = e d_{ab} \sqrt{\frac{2\pi\omega_{\mathbf{p}}}{\epsilon L_w}} \varphi_{1s}(0)\Phi_{\alpha,\mathbf{p}}, \tag{4}$$

where d_{ab} is the dipole matrix element. The dispersion for photons in a microcavity of width L_w is given by $\omega_{\mathbf{p}} = \sqrt{\omega_0^2 + (c\mathbf{p})^2/\epsilon}$, where $\omega_0 = 2\pi c/L_w\sqrt{\epsilon}$, and can be approximated, for small momenta, by a parabolic dispersion $\omega_{\mathbf{p}} \simeq \omega_0 + \mathbf{p}^2/2m_{ph}$, with the photon mass given by $m_{\mathrm{ph}} = 2\pi\sqrt{\epsilon}/cL_w$.

Because there may be many different exciton wave functions corresponding to similar exciton energies, the oscillator strength $g_{\alpha,\mathbf{p}}$ is a random quantity, which varies both in phase and magnitude. Considering many disorder realizations, we find a distribution of squared oscillator strengths $|g_{\alpha,\mathbf{p}}|^2$ as a function of the energy ε_α and momentum $\mathbf{p}$. This distribution reflects the statistical properties of the center of mass excitonic wave functions.

To compare to experimentally relevant observables, we introduce the density of states (DOS),

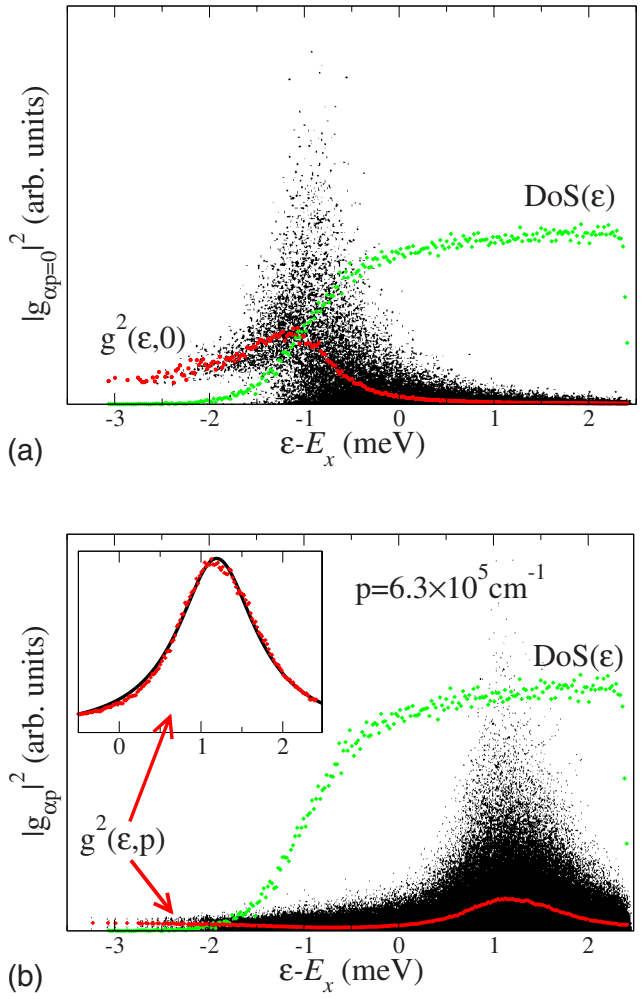

FIG. 2. (Color online) Plot showing the energy dependence of the excitonic squared coupling strength $|g_{\alpha,\mathbf{p}}|^2$ on photons of momentum (a) $|\mathbf{p}| = 0$ (from Ref. 25, for comparison) and (b) $|\mathbf{p}| = 6.3 \times 10^5\ \mathrm{cm}^{-1}$, where all exciton states are found numerically. Results are taken from 160 different realizations of disorder potential, and for (b), coupling strengths from eight different photon momenta (p_x, p_y) with the same value of $|\mathbf{p}|$ are combined. The mean squared averaged oscillator strength $g^2(\varepsilon, |\mathbf{p}|)$ for the same value of momentum [lower red (gray) points] and the density of states DOS(ε) [upper green (gray) points] are also explicitly plotted. Inset: Fit of $g^2(\varepsilon, |\mathbf{p}|)$ to expression (7) with a renormalized energy $\varepsilon_{\mathbf{p}}$.

$$\mathrm{DOS}(\varepsilon) \equiv \frac{1}{L^2}\sum_\alpha \langle \delta(\varepsilon - \varepsilon_\alpha)\rangle,$$

and the mean squared oscillator strength,

$$g^2(\varepsilon, |\mathbf{p}|) = \frac{1}{\mathrm{DOS}(\varepsilon)}\left\langle \sum_\alpha |g_{\alpha,\mathbf{p}}|^2 \delta(\varepsilon - \varepsilon_\alpha)\right\rangle, \tag{5}$$

where $\langle \ldots \rangle$ is the average over different disorder realizations. These quantities are related to the excitonic optical density by the relation

$$D(\varepsilon) = \mathrm{DOS}(\varepsilon) g^2(\varepsilon, 0). \tag{6}$$

Experimentally, the excitonic optical density can be measured by dividing the PL emission by the excitonic occupation.[34] We note that in the noncondensed regime, the full distribution of $g_{\alpha,\mathbf{p}}$ is unnecessary; the excitonic optical density is sufficient to derive the polariton dispersion and its inhomogeneous broadening. However, in the condensed phase, and in order to correctly describe resonant Rayleigh scattering mechanisms, we will see that it is of fundamental importance to consider the full distribution of oscillator strengths.

Focusing for the moment on average properties, rather than on the entire distribution, a simple expression exists for the mean squared oscillator strength in the high-energy limit. In this limit, where the DOS is flat and energy independent, $\mathrm{DOS}(\varepsilon) \simeq \nu$, making use of the Born approximation, the squared average oscillator strength $g^2(\varepsilon, |\mathbf{p}|)$ does not depend separately on the disorder potential correlation length ℓ_c and variance σ, but instead depends only on the scattering time τ (see Fig. 2):

$$g^2(\varepsilon, |\mathbf{p}|) \simeq \frac{1}{m_x \tau L^2} \frac{1}{(\varepsilon - \varepsilon_{\mathbf{p}})^2 + (1/2\tau)^2}, \tag{7}$$

where $\varepsilon_{\mathbf{p}} = E_x + \mathbf{p}^2/2m_x$ is the free particle dispersion. From this form, and the effectively constant density of states, one can see that both the mean squared oscillator strength and the excitonic optical density are symmetrical. The comparison of this approximate form to the numerical simulation is shown in Fig. 2;

In contrast, for energies much below the band edge, the specific asymptotic expression of $g^2(\varepsilon, |\mathbf{p}|)$ depends on whether the correlation length ℓ_c is smaller or larger than the localization length $r_\Phi(\varepsilon)$. In the white noise limit,[45] $\ell_c \ll r_\Phi(\varepsilon) \sim (2m_x|\varepsilon - E_x|)^{-1/2}$, one can show that the center of mass wave function $\Phi_\alpha(\mathbf{R})$ can be approximated by a Gaussian centered at a randomly distributed site $\mathbf{R}_\alpha$,

$$\Phi_\alpha(\mathbf{R}) = r_\Phi^{-1} e^{-(\mathbf{R} - \mathbf{R}_\alpha)^2 / r_\Phi^2},$$

$$\Phi_{\alpha,\mathbf{p}} = r_\Phi e^{i\mathbf{p}\cdot\mathbf{R}_\alpha - (r_\Phi \mathbf{p})^2/4},$$

and, therefore, give a squared oscillator strength proportional to

$$|\Phi_{\alpha,\mathbf{p}}|^2 \simeq \frac{1}{2m_x|\varepsilon - E_x|} e^{-|\mathbf{p}|^2/(4m_x|\varepsilon - E_x|)}.$$

Thus, here the distribution of squared oscillator strengths is very narrow, with a mean square value given by the above form.

Similarly, much theoretical (and numerical) work has been done to establish the energy dependence of the density of states. In the low-energy tail, as before, the specific asymptotic form of the DOS depends on the value of the correlation length ℓ_c. In the white noise limit, one can show that $\mathrm{DOS}(\varepsilon) \propto |\varepsilon - E_x|^{3/2} e^{-11.8|\varepsilon - E_x|/\sigma^2 m_x \ell_c^2}$, while in the opposite (classical) limit, $\ell_c \gg r'_\Phi(\varepsilon) \sim (2\ell_c/\sqrt{2m_x|\varepsilon - E_x|})^{1/2}$, one, instead, has $\mathrm{DOS}(\varepsilon) \propto (\varepsilon - E_x)^2 e^{-(\varepsilon - E_x)^2/2\sigma^2}$ (see, e.g., Ref. 43). In general, for the finite values of the disorder correlation length corresponding to typical experiments, the regions in energy where one of these two analytical regimes applies are very restricted, and therefore, a numerical analysis is required.

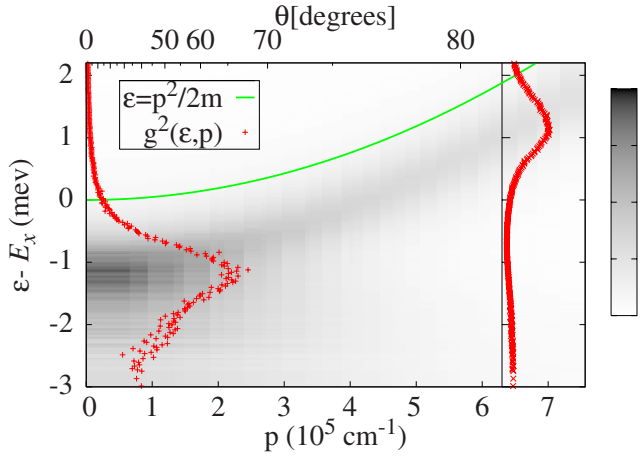

FIG. 3. (Color online) Contour plot of the mean (over 160 realizations of the disorder potential) squared oscillator strength $g^2(\varepsilon, |\mathbf{p}|)$ versus energy and momentum [or, equivalently, angle $\theta = \tan^{-1}(c|\mathbf{p}|/\omega_0)$]. Note that the scale in angle is not linear. The free particle dispersion $E_x + |\mathbf{p}|^2/2m_x$ [solid green (gray) line] and the trace of the mean squared oscillator strength for two representative values of momenta, $|\mathbf{p}| = 0$ ($\theta = 0°$) and $|\mathbf{p}| = 6.3 \times 10^5$ cm^{-1} ($\theta = 82°$) [red (gray) plus symbols] are explicitly plotted (cf. Fig. 2). The figure is adapted from Ref. 25.

Numerical analysis is also essential in order to account for the distribution of squared oscillator strengths $|g_{\alpha,\mathbf{p}}|^2$ near the band edge. This distribution changes substantially from low-energy states to high-energy ones. As we discuss in more detail in the next section, for high-energy states, the oscillator strength distribution is governed by a Porter-Thomas law, while for Lifshitz tail states, the distribution follows a narrow Gaussian-like distribution. Neither of these distributions

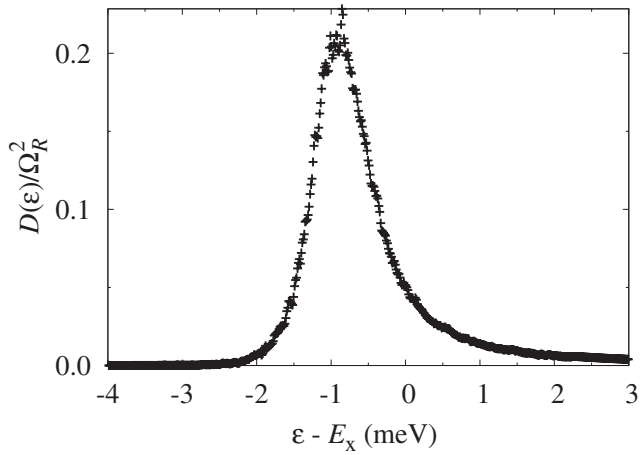

FIG. 4. Optical density Eq. (6) versus energy. The maximum value is around $\varepsilon^* - E_x \simeq -0.94$ meV and the FWHM $\sigma^* \simeq 0.94$ meV.

applies for energies around the band edge. However, it is those states near the band edge that have the largest optical density, and so the distribution of oscillator strengths in this region has a significant impact on derived quantities. It thus becomes essential to use numerical analysis to find the entire distribution of oscillator strengths.

B. Numerical analysis

To solve Eq. (3), we exactly diagonalize this problem within a finite basis set using conjugate-gradient minimization with preconditioning of the steepest descent wave vector (for a detailed discussion of this method, see Ref. 46). We find the exact eigenvalues and eigenfunctions in a finite basis on a grid of 120×120 points for a system of size $L=1$ μm, $\sigma=2$ meV, $\ell_c=166$ Å, and excitonic mass $m_x/m_0=0.08$. These parameters give an inverse scattering time of $1/\tau=1.16$ meV. For this choice of the grid, one can show that convergence is reached. From the evaluated eigenvalues ε_α and eigenstates $\Phi_{\alpha,\mathbf{p}}$ over 160 realizations of the disorder potential, we can derive the excitonic density of states and the oscillator coupling strength and its squared average [Eq. (5)], which we plot in Figs. 2 and 3, while the corresponding optical density is plotted in Fig. 4.

The lower panel of Fig. 2 shows the squared coupling strength $|g_{\alpha,\mathbf{p}}|^2$ versus energy for a fixed value of momentum, $|\mathbf{p}|=6.3\times10^5$ cm^{-1}, corresponding, for a cavity of $\omega_0=1.68$ eV, to an angle of $\theta=\tan^{-1}(c|\mathbf{p}|/\omega_0)=82°$. Note that, because of the presence of disorder in the quantum well, one photon with a given momentum couples with many exciton states with different energies. We will see later on, therefore, that a polariton with a given momentum is formed by the superposition of one photon state $|\mathbf{p}\rangle$ and many exciton states $|\Phi_\alpha\rangle$. These states are more or less strongly coupled, depending on the distribution of oscillator strength for that given momentum. As Fig. 2 shows, by probing a quantum well at a large angle, i.e., with high momenta photons, the excited excitons with larger oscillator strength are the ones that are almost delocalized in nature and with a many-node fractal-like shape. By taking the average over many (160) disorder realizations, the squared average oscillator strength $g^2(\varepsilon,|\mathbf{p}|)$ shown in the inset in Fig. 2 is well described by the Lorentzian shape predicted by the Born approximation of Eq. (7), with a fitted width of $1/\tau_{\mathrm{fit}}\simeq1.2$ meV in good agreement with the theoretical value $1/\tau=1.16$ meV. However, the peak of the Lorentzian does not coincide with the energy of the clean limit, $\varepsilon_{\mathbf{p}}$, but is renormalized down in value, as can be shown by employing a self-consistent Born approximation.

In contrast, as shown in the upper panel of Fig. 2, for photons with zero momentum, the maximum value of the oscillator strength characterizes excitonic states below the band edge, which are more localized in nature. This can be easily understood by the following qualitative argument: At very low energies, the excitonic state is strongly localized in a deep potential minimum and has no nodes. Increasing the energy, at first the localization length increases [e.g., $r_\Phi(\varepsilon)\sim(2m_x|\varepsilon-E_x|)^{-1/2}$ in the white noise limit] and, thus, increases the oscillator strength. However, eventually, the wave function starts developing nodes and consequently, the squared average oscillator strength decreases. When $\mathbf{p}=0$, only the high-energy side of $g^2(\varepsilon,0)$ can be described by the Born limit [Eq. (7)]. For the chosen values of the disorder potential correlation length ℓ_c and variance σ, an analytical expression for the low-energy (Lifshitz) tail is not known.

The crossover from localized to more plane-wave-like excitonic states obtained by increasing the value of the photon momentum is plotted in Fig. 3. At high momenta, the maximum of the squared average oscillator strength $g^2(\varepsilon,|\mathbf{p}|)$ shown in Fig. 3 follows the free particle dispersion, plus a renormalization down in energy, which decreases for higher photon momenta; i.e., these states are described well by free particles, including disorder in the first Born approximation. At low momenta, the states which have the stronger oscillator strength are effectively localized. The crossover, as seen in the contour plot, happens at relatively large angle, $\theta\simeq55°$, because of the large ratio of exciton to photon mass: The crossover momentum is set by exciton mass, but its conversion to an angle depends on effective photon mass. For a related reason, the thermally populated polariton states are formed out of strongly localized (i.e., beyond first Born approximation) excitonic states. For values of temperature and photon mass relevant for experiments, thermal population of polaritons extends up to around 10° in momentum, which, as seen in Fig. 3, corresponds to exciton states not accurately described by the Born approximation. For this reason, in the following, we will concentrate on the oscillator strength corresponding to $\mathbf{p}\simeq0$, $|g_{\alpha,0}|^2$.

Finally, we plot in Fig. 4 the optical density. For the chosen values of ℓ_c and σ, the optical density shows a maximum around $\varepsilon^*-E_x\simeq-0.94$ meV below the band edge, a full width at half maximum (FWHM) of approximatively $\sigma^*\simeq0.94$ meV, and a clear asymmetry of the line shape. It is well known[32,44] that, by indicating with $E_c=1/2m_x\ell_c^2$ the confinement energy of the lowest state in a typical potential minimum, the excitonic line shape is determined by the ratio E_c/σ and, for a finite value of this, the optical density develops an asymmetry toward higher energies. For our choices of parameters, $E_c/\sigma\simeq0.85$. Asymmetry of the optical density of quantum well excitons has also been measured experimentally (see, e.g., Ref. 34) by dividing the measured PL by the excitonic occupation.

As mentioned earlier, the full distribution of oscillator strengths, and not just its mean squared value, will be important. It is useful to discuss here some technical details of how this is extracted. The numerical analysis provides the excitonic eigenvalues and eigenstates only within a finite interval in energy. (The lowest energy states arise from rare potential fluctuations, which would require a larger region of space to be sampled; the highest energy states have spatial variation on length scales finer than our grid.) Within the interval of energies found, averages are performed by making use of the raw data coming from 160 realizations of the disorder potential; outside this interval, averages are taken by extrapolating the numerics. In particular, in the low-energy Lifshitz tail, as the oscillator strengths have a narrow Gaussian distribution around its squared averaged value, we approximate the distribution of $|g_{\alpha,0}|^2$ with a delta function at its extrapolated value $g^2(\varepsilon,0)$. In the very high energy region, instead, we make use of the Porter-Thomas distribution,

$$\mathcal{P}(x=|g_{\alpha,0}|^2)=\frac{\exp[-x/(2\bar{x})]}{\sqrt{2\pi x\bar{x}}},$$

where $\bar{x}=g^2(\varepsilon,0)$, again extrapolating the fitted value for the squared averaged oscillator strength. In addition, we fix the overall scale of $|g_{\alpha,0}|^2$ to match integrated optical intensity with half the experimentally measured Rabi splitting Ω_R squared:

$$\int d\varepsilon D(\varepsilon)=\frac{\Omega_R^2}{4}. \tag{8}$$

This normalization accounts for factors other than the wavefunction in Eq. (4).

C. Mean-field theory

In the remainder of this paper, we will discuss optical probes, with particular emphasis on resonant Rayleigh scattering. Such optical responses are described by considering fluctuations about the mean-field theory. Thus, to establish our notation, in this section we will briefly summarize the mean-field theory of the model in Eq. (1); this mean-field theory has been discussed in detail elsewhere.[17,40] As well as describing the optical response, fluctuations about the mean-field theory can also be important in describing, in the extremely low-density limit, corrections to the mean-field thermodynamics. Since the subject of this paper is optical probes, we will not discuss the subject of fluctuation corrections to the critical temperature here, as they have been discussed elsewhere.[21]

We consider a thermal equilibrium system of polaritons, with total density fixed by introducing a chemical potential μ. Making use of standard path integral techniques, and integrating out the fermionic fields, the partition function may be written in terms of the imaginary time action:

$$S[\psi]=\int_0^\beta d\tau\sum_{\mathbf{p}}\psi_{\mathbf{p}}^*(\partial_\tau+\tilde{\omega}_{\mathbf{p}})\psi_{\mathbf{p}}-\mathrm{Tr}\ln G^{-1}. \tag{9}$$

Here, G^{-1} is the energy level diagonal, inverse single-particle Green's function:

$$G_\alpha^{-1}=\begin{pmatrix}\partial_\tau+\tilde{\varepsilon}_\alpha/2 & \sum_{\mathbf{p}} g_{\alpha,\mathbf{p}}\psi_{\mathbf{p}}/\sqrt{N}\\ \sum_{\mathbf{p}} g_{\alpha,\mathbf{p}}^*\psi_{\mathbf{p}}^*/\sqrt{N} & \partial_\tau-\tilde{\varepsilon}_\alpha/2\end{pmatrix}, \tag{10}$$

where $\tilde{\varepsilon}_\alpha=\varepsilon_\alpha-\mu$ and $\tilde{\omega}_{\mathbf{p}}=\omega_{\mathbf{p}}-\mu$ are respectively the excitonic and photonic energies measured with respect to the chemical potential.

Although the quantum well excitons are disorder localized, for a weak disorder potential, with $\sigma<\Omega_R$, and in the absence of strong photon disorder (which in some cases can also be relevant[38,47]), the resultant polaritons are delocalized. As such, polaritons will be described by a momentum quantum number and condense, as in the usual picture, in the lowest momentum state. The mean-field theory of such a state is described by the static and uniform minimum $\psi_{\mathbf{p}}(\tau)=\psi\delta_{\mathbf{p},0}$ of the action (9) (or saddle-point equation), which has to be solved together with the mean-field equation for the total number of excitations (2):

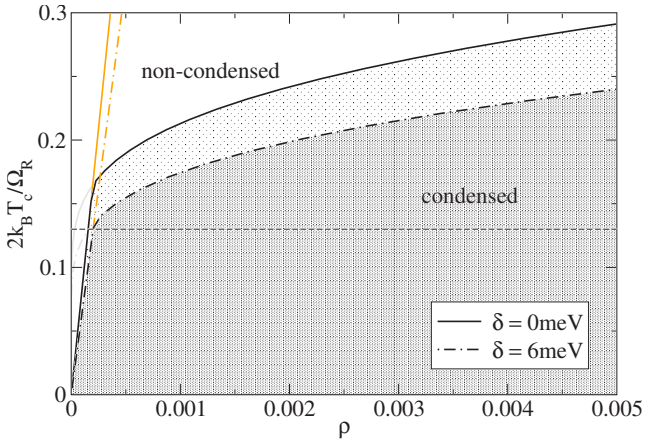

FIG. 5. (Color online) Phase diagram for the dimensionless critical temperature $2k_BT_c/\Omega_R$ versus the dimensionless density ρ for effective zero detuning $\delta=\omega_0-\varepsilon^*=0$ meV (ε^* is the energy at which the excitonic optical density has its maximum, and so as seen in Fig. 4, $\delta=0$ implies $\omega_0-E_x=-0.94$ meV) (solid black) and for positive detuning $\delta=+6$ meV ($\omega_0-E_x=+5.06$ meV) (dotted-dashed black) and $\Omega_R=26$ meV. The mean-field boundaries for the two different detunings are cut off by the expected linear dependence of the critical temperature, as indicated at extremely low densities [orange (gray) solid and dotted-dashed lines]. The horizontal dashed line marks the temperature of $k_BT=20$ K, which will be used in later figures.

$$\tilde{\omega}_0=\frac{1}{N}\sum_\alpha|g_{\alpha,0}|^2\frac{\tanh\beta E_\alpha}{2E_\alpha}, \tag{11}$$

$$\rho=\frac{1}{N}\psi^2+\frac{1}{N}\sum_\alpha\left[\frac{1}{2}-\frac{\tilde{\varepsilon}_\alpha\tanh\beta E_\alpha}{4E_\alpha}\right]. \tag{12}$$

Here, E_α is the energy of an exciton in the presence of a coherent photon field and is given by

$$E_\alpha=\sqrt{(\tilde{\varepsilon}_\alpha/2)^2+|g_{\alpha,0}|^2\psi^2/N}. \tag{13}$$

In Fig. 5, the mean-field critical density is shown. Over the range of densities shown, the appearance of this mean-field phase boundary does not differ significantly from the mean-field results of previous work,[17] in which the DOS was taken to be a Gaussian and, moreover, where the coupling strength was kept fixed. Despite the similarity of appearance, there are two differences that the realistic distribution of energies and oscillator strengths introduces: it gives an absolute scale for the density and it affects the mean-field phase boundary at very large densities.

The effect of coupling strength distribution on the density scale can be understood as follows. By solving the "gap equation" Eq. (11) in the limit $\psi\to 0$, one finds T_c as a function of the chemical potential μ, forgetting about the corresponding excitation density. At the phase boundary, where $\psi=0$, the squared oscillator strength appears only linearly in Eq. (11), so this expression depends only on the optical density $D(\varepsilon)$. By taking into account the density equation (12),

the critical temperature can be expressed as a function of the excitation density rather than as a function of the chemical potential. This translation to densities makes use of the density of states. In the standard BCS theory, and in Ref. 17, there is no modulation of the interaction strength and, therefore, no difference between optical density $D(\varepsilon)$ and density of states $\mathrm{DOS}(\varepsilon)$. In our system, the asymptotic forms of the optical density and the density of states do not match. This difference of asymptotic forms is important in measuring the density in physical units.

The asymptotic form of the phase boundary at large densities (well beyond the range shown in Fig. 5 and beyond the validity of our model) is controlled by the fact that the density of states asymptotes to a constant at large densities, and the presence of those exciton states that couple only weakly to light. At smaller densities, such states have little effect on the phase boundary.

III. OPTICAL PROBES

The optical absorption and emission spectra of a microcavity can be derived by first finding the Green's function describing photon propagation. The noncondensate part of these response functions (i.e., away from zero momentum) may be found, in practice, by considering the Green's function for fluctuations about the mean-field solution, $\psi_{\mathbf{p},\omega_h} = \psi\delta_{\mathbf{p},0}\delta_{\omega_h,0} + \delta\psi_{\mathbf{p},\omega_h}$, where $\omega_h = 2\pi h/\beta$ are bosonic Matsubara frequencies, and by expanding the action (9) up to quadratic terms:

$$\delta S \simeq \frac{\beta}{2}\sum_{\omega_h,\mathbf{p},\mathbf{q}} \begin{pmatrix} \delta\psi^*_{\omega_h,\mathbf{p}} \\ \delta\psi_{-\omega_h,-\mathbf{p}} \end{pmatrix}^T \mathcal{G}^{-1}_{\mathbf{pq}}(\omega_h) \begin{pmatrix} \delta\psi_{\omega_h,\mathbf{q}} \\ \delta\psi^*_{-\omega_h,-\mathbf{q}} \end{pmatrix}.$$

This gives the Matsubara inverse photonic Green's function:

$$\mathcal{G}^{-1}_{\mathbf{pq}}(\omega_h) = \begin{pmatrix} K^{(1)}_{\mathbf{pq}}(\omega_h) & K^{(2)}_{\mathbf{pq}}(\omega_h) \\ K^{(2)}_{\mathbf{pq}}(\omega_h) & K^{(1)*}_{\mathbf{qp}}(\omega_h) \end{pmatrix}.$$

Physical response functions can be found by analytic continuation of the imaginary time Matsubara Green's function to real times.[48] The matrix elements of $\mathcal{G}^{-1}_{\mathbf{pq}}(\omega_h)$ can be expressed in terms of the bare photon energy $\omega_{\mathbf{p}}$ and the excitonic quasiparticle energy E_α as follows:

$$K^{(1)}_{\mathbf{pq}}(\omega_h) = \delta_{\mathbf{p},\mathbf{q}}(i\omega_h + \tilde{\omega}_{\mathbf{p}}) + \frac{1}{N}\sum_\alpha g^*_{\alpha,\mathbf{p}} g_{\alpha,\mathbf{q}} \frac{\tanh(\beta E_\alpha)}{E_\alpha} \frac{i\omega_h\tilde{\varepsilon}_\alpha/2 - E^2_\alpha - (\tilde{\varepsilon}_\alpha/2)^2}{\omega_h^2 + 4E^2_\alpha} - \delta_{\omega_h,0}\frac{1}{N}\sum_\alpha \gamma_{\alpha,\mathbf{p},\mathbf{q}}, \tag{14}$$

$$K^{(2)}_{\mathbf{pq}}(\omega_h) = \frac{1}{N}\sum_\alpha |g_{\alpha,0}|^2 g^*_{\alpha,\mathbf{p}} g_{\alpha,\mathbf{q}} \frac{\psi^2}{N} \frac{\tanh(\beta E_\alpha)}{E_\alpha} \frac{1}{\omega_h^2 + 4E^2_\alpha} - \delta_{\omega_h,0}\frac{1}{N}\sum_\alpha \gamma_{\alpha,\mathbf{p},\mathbf{q}}, \tag{15}$$

where

$$\gamma_{\alpha,\mathbf{pq}} = \beta|g_{\alpha,0}|^2 g^*_{\alpha,\mathbf{p}} g_{\alpha,\mathbf{q}} \frac{\psi^2}{N} \frac{\mathrm{sech}^2(\beta E_\alpha)}{4E^2_\alpha}.$$

It is useful to decompose the photonic Green's function into its momentum-diagonal and off-diagonal contributions:

$$K^{(1,2)}_{\mathbf{pq}}(\omega_h) = K^{(1,2)}_{\mathbf{pp}}(\omega_h)\delta_{\mathbf{p},\mathbf{q}} + K^{(1,2)o}_{\mathbf{pq}}(\omega_h). \tag{16}$$

By treating the off-diagonal terms perturbatively, the translational invariance can be recovered and polariton eigenstates can be labeled by momentum vectors. In the next section, we will focus on the diagonal terms, which characterize both the spectral weight and the photoluminescence emission. Section III C is then dedicated to RRS, for which we will see that the off-diagonal terms are necessary in order to describe the scattering of an incident photon (via the excitonic component of the microcavity polariton mode) into directions other than its original direction.[35]

A. Spectral weight and photoluminescence

Secondary emission from a semiconductor microcavity after optical excitation is the source of both incoherent PL and coherent RRS. At short times, this emission is dominated by RRS, the coherent scattering from disorder, and so is at the energy of, and coherent with, the incident radiation. At longer times, phonon and particle-particle scattering destroy coherence and redistribute the energy, leading to a quasiequilibrium distribution of energies, and thus, the incoherent PL emission intensity,

$$P(\omega,\mathbf{p}) = n_B(\omega)W(\omega,\mathbf{p}), \tag{17}$$

is given by the Bose occupation factor $n_B(\omega)$ times the spectral weight:

$$W(\omega,\mathbf{p}) = 2\Im G^{11}_{\mathbf{pp}}(\omega_h)|_{i\omega_h=-\omega-i\eta}. \tag{18}$$

The spectral weight can be interpreted as an absorption coefficient[21] (the probability to absorb a photon minus the probability to emit a photon), where negative values of $W(\omega,\mathbf{p})$ represent gain. In contrast, the PL $P(\omega,\mathbf{p})$ is always positive.

In calculating the PL, it is convenient to make an approximation by neglecting multiple polariton scattering while still including the effects of exciton-disorder scattering to all orders. This is discussed in Ref. 33, where comparison between this approximation and exact numerical calculations show this approximation to be remarkably good. Physically, this is a good limit to consider because the typical exciton-disorder scattering times are very short compared to the inverse frequencies considered in PL. As PL depends on the momentum-diagonal part of the photon Green's function, neglect of multiple scattering means, in practice, averaging over disorder realizations at the level of the inverse photon Green's function, $\mathcal{G}^{-1}_{\mathbf{pq}}(\omega_h)$. Since off-diagonal terms in the inverse Green's function [Eq. (16)] break translational invariance, they average to zero, and so scattering between different photon momentum states can, thus, be neglected. The off-diagonal terms neglected here will, however, play a crucial role in the case of RRS response, as discussed below.

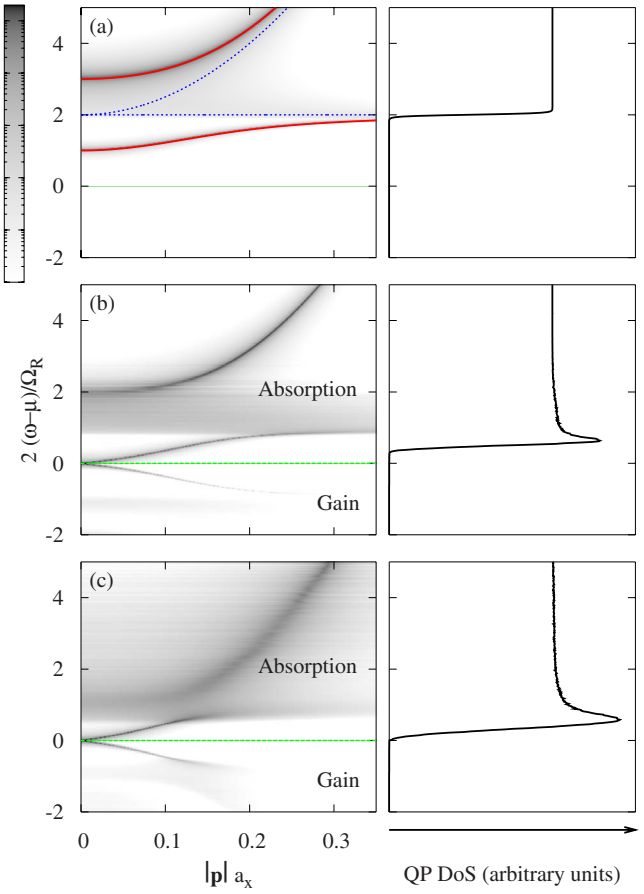

FIG. 6. (Color online) Left column: Contour plot of the spectral weight $W(\omega,\mathbf{p})$ as a function of the dimensionless momentum $|\mathbf{p}|a_x$ and rescaled energy $2(\omega-\mu)/\Omega_R$, for zero detuning $\delta=\omega_0-\varepsilon^*=0(\omega_0-E_x=-0.94$ meV), $\Omega_R=26$ meV, $k_BT=20$ K, and photon mass $m_{\mathrm{ph}}\Omega_R a_x^2/2=0.01$. Right column: Plot of the quasiparticle DOS for the same choice of parameters as the left column, respectively: (a) noncondensed ($\rho\simeq 0$, $E_x-\mu\simeq 27$ meV) (the bare exciton and photon dispersions [blue (dark gray) dotted line] and the upper and lower polariton dispersions [red (gray) solid line] obtained from the effective coupled oscillator model are shown for comparison), (b) condensed ($\rho\simeq 7.8\times 10^{-3}$, $E_x-\mu\simeq 11$ meV), and (c) condensed ($\rho\simeq 6.7\times 10^{-2}$, $E_x-\mu\simeq 7$ meV).

The spectral weight calculated from this formula, along with the quasiparticle density of states, is shown in Fig. 6. We first discuss this in the noncondensed case, where $\psi=0$, and so $K^{(2)}_{\mathbf{pq}}(\omega_h)=0$, and the photon's Green function becomes diagonal in particle-hole space and simplifies to

$$\mathcal{G}^{-1}_{\mathbf{pp}}(\omega_h)\simeq i\omega_h+\tilde{\omega}_{\mathbf{p}}-\int_{-\infty}^{\infty}d\varepsilon D(\varepsilon)\frac{\tanh(\beta\tilde{\varepsilon}/2)}{i\omega_h+\tilde{\varepsilon}}.$$

This expression describes the coupling of one harmonic oscillator (the photon mode) to many harmonic oscillators (the exciton modes). In the limit of small density, the chemical potential is far below all exciton modes, and so $\tanh(\beta\tilde{\varepsilon}/2)\simeq 1$. In this limit, the result is identical to a bosonic description of excitons, sometimes also called the *linear dispersion model*. The underlying fermionic structure appears as a reduction of the effective exciton-photon coupling, due to saturation effects described by the $\tanh(\beta\tilde{\varepsilon}/2)$ term, and is discussed in more detail below.

From this linear dispersion model, describing one oscillator coupled to many, there are, in general, two broadened modes at high and low energies—here, these are the lower polariton (LP) and upper polariton (UP)—and a continuum of modes associated with the exciton optical density. However, when considering the corresponding spectral weight, modes are weighted by their photonic component, so one primarily sees the LP and UP modes, and only weak emission near the bare excitonic states—the excitonic "dark" states. These three features are clearly visible in Fig. 6 and have been previously predicted by Houdré *et al.*,[49] making use of a simplified and exactly solvable model. Note that in the limit of an infinitely narrow spectral width, these dark exciton states become entirely dark, having vanishing photon component. The presence of dark exciton states coexisting with strong coupling polaritons can explain the simultaneous observation of large Rabi splittings and long decay times seen in some experiments.[50]

When the Rabi splitting is substantially larger than the exciton inhomogeneous broadening (in our case we have $\Omega_R=26$ meV and the FWHM of the optical density $\sigma^*=0.94$ meV), there is a substantial difference between broadening of lower and upper polaritons. This is because the high-energy tail of the optical density decays as a power law, while the low-energy Lifshitz tail decays exponentially. Thus, the optical density has a larger value at the UP mode than at the LP mode, giving a larger broadening compared to the almost vanishing width of the LP. This description of the polariton linewidth due to the excitonic inhomogeneous broadening coincides with that of Whittaker,[33] and it has been well tested experimentally.[34]

In addition, the location of the LP and UP can be found by making use of an effective two-oscillator model, i.e., assuming a narrow deltalike optical density,

$$D(\varepsilon)\mapsto\left(\frac{\Omega_R}{2}\right)^2\delta(\varepsilon-\varepsilon^*),$$

where ε^* is the location of the maximum optical density and, effectively, the exciton energy. In this case, the system reduces to two coupled oscillators, giving unbroadened LP and UP poles at

$$E_{\mathrm{LP,UP}}=\frac{\tilde{\omega}_{\mathbf{p}}+\tilde{\varepsilon}^*}{2}\pm\frac{1}{2}\sqrt{(\tilde{\omega}_{\mathbf{p}}-\tilde{\varepsilon}^*)^2+\bar{\Omega}_R^2},\qquad(19)$$

where $\bar{\Omega}_R^2\equiv\Omega_R^2\tanh(\beta\tilde{\varepsilon}^*/2)$ is the reduced Rabi splitting, due to saturation effects at higher densities. The reduction of $\bar{\Omega}_R$ splitting, thus, translates directly into a reduction of the LP-UP splitting, and thus, a blueshift of the LP, which at small densities can be shown to be linear. For comparison, the results of this formula are shown by the solid (red) lines in Fig. 6(a). In Sec. III B, we will discuss the calculation of this linear blueshift in the low-density regime by evaluating $\bar{\Omega}_R$ as a function of density, making use of the full density of states.

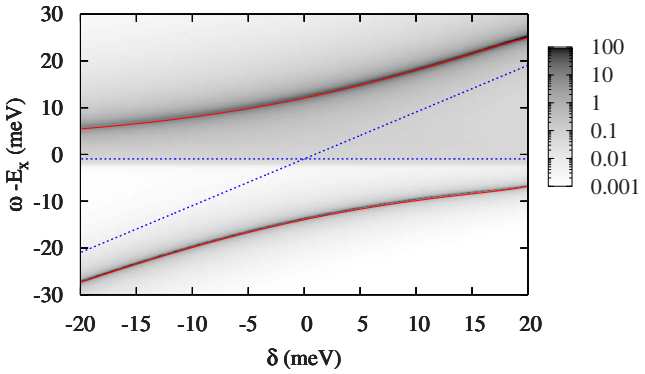

FIG. 7. (Color online) Contour plot of the spectral weight $W(\omega,0)$ for $\mathbf{p}=0$ as a function of the detuning $\delta=\omega_0-\varepsilon^*$ and energy $\omega-E_x$, for a fixed and very low value of density ($\rho\simeq 0$, $E_x-\mu \simeq 27$ meV) and $k_BT=20$ K ($2k_BT/\Omega_R=0.13$). The bare exciton and photon dispersions [blue (dark gray) dotted line] and the upper and lower polariton dispersions [red (gray) solid line] obtained from the effective coupled oscillator model are explicitly shown.

Let us now turn to the signatures of condensation as seen in the spectral weight, and thus, in the PL emission (but which are most probably masked in the PL emission by strong emission from the condensate mode). When condensed, the polariton modes are replaced by new collective modes:[21,25] The lower polariton becomes the linear Goldstone mode, and two branches appear below the chemical potential. The appearance of new excitation branches below the chemical potential is generic to condensation;[51] however, the experiments required to probe these modes are not easy in other Bose condensed systems, such as atomic gases. For this reason, let us briefly discuss the physical origin of these new branches and the reason why they may be observed in optical response of polariton systems. The Bogoliubov spectrum arises because of the possibility of processes that spontaneously either create or destroy two noncondensed particles. (Such processes arise due to scattering from or to the condensate.) As a result of these processes, there is mixing between the propagation of an extra particle or propagation of a missing particle (i.e., a hole). (Such a language of particle and hole refers to the normal state quasiparticles; in the current case, the normal state polaritons.) In the normal state, one can separately calculate the spectral weight of particle excitations, which have weight only above the chemical potential, and hole excitations, which have weight only below the chemical potential. When condensed, as the "particle" and "hole" spectral weights become mixed, this mixing can lead to a spectral weight below the chemical potential that is associated with particle propagation. To observe this weight, it is, however, necessary to have the ability to inject a particle which is not a quasiparticle of the condensed system, i.e., not a Bogoliubov quasiparticle. In atomic experiments, this is hard to achieve, but for polaritons can be naturally achieved by injecting a photon. These new branches below the chemical potential are seen as optical gain in the spectral weight (see Fig. 6). Note that the presence of pumping and decay will modify the linear dispersion of the Goldstone mode at low momentum, making it diffusive,[26] and that quantization by disorder may also have some effect.[52]

The spectral weight also contains information about the excitonic quasiparticle DOS of the system. As discussed above for the noncondensed case, this is visible via the appearance of dark exciton states [see Figs. 7 and 6(a)]. When condensed, there is a coherent field that modifies the energies of these excitonic quasiparticle states, as given in Eq. (13), and thus modifies their density of states. The density of states given by taking the energy of such modes is shown by the right column of Fig. 6, and can be compared to the corresponding faint features seen in the photon spectral weight in the left column.

The change to the quasiparticle density of states that occurs on condensation requires some explanation. As mentioned earlier, the change of this spectrum is similar to that seen in the BCS theory of superconductivity, as such it is surprising that there is no gap in the density of states of Fig. 6. In fact, there would be a gap if the distribution of oscillator strengths were replaced with the mean square oscillator strength. In that case, there would be a branch cut and a $(E-g\psi/\sqrt{N})^{-1/2}$ singularity in the density of states. However, with the full distribution of oscillator strengths, one finds that there is always a nonvanishing probability of arbitrarily small oscillator strengths. (Note that if the oscillator strength were zero, the corresponding state would not contribute to any photon response, but for an arbitrarily small coupling, it has some contribution.) Thus, the contribution of these weakly coupled exciton states in effect smoothes out the gap. Thus, this system can be vaguely described as "gapless fermion condensation," analogous to "gapless superconductivity" but through a mechanism very different from the standard Abrikosov-Gor'kov mechanism considered in superconductors.[18,48]

As one moves away from the chemical potential, the mixing of particle and hole modes described by the Bogoliubov spectrum decreases. As a result, far above the chemical potential, the modes are the same as the uncondensed case, and far below the chemical potential, the new modes disappear. To explain this quantitatively, it is clearer to discuss the case of weakly interacting Bose gas.[51] Writing the Bogoliubov mode energy as $\xi_{\mathbf{p}}=\sqrt{\epsilon_{\mathbf{p}}(\epsilon_{\mathbf{p}}+2\mu)}$, where $\mu=g\psi^2$ is the mean-field value, the spectral weight is given by

$$W(\omega,\mathbf{p})=\frac{\epsilon_{\mathbf{p}}+\mu+\xi_{\mathbf{p}}}{2\xi_{\mathbf{p}}}\delta(\omega-\xi_{\mathbf{p}})-\frac{\epsilon_{\mathbf{p}}+\mu-\xi_{\mathbf{p}}}{2\xi_{\mathbf{p}}}\delta(\omega+\xi_{\mathbf{p}}).$$

It is, thus, clear that at large momenta, where $\xi_{\mathbf{p}}\simeq\epsilon_{\mathbf{p}}+\mu$, the coefficient of the first delta function (modes above the chemical potential) will approach 1, and the coefficient of the second (modes below) will be suppressed to zero (roughly quadratically in energy).

In contrast to the power law suppression of the spectral weight of modes far below the chemical potential, the PL signal from modes far above zero is suppressed exponentially by the thermal occupation of these modes [see Eq. (17)], while below the chemical potential, there is no such decay. However, this discussion neglects emission from the condensate mode, which should be included at zero momentum, as defined in Eq. (17). To see a noticeable change of the

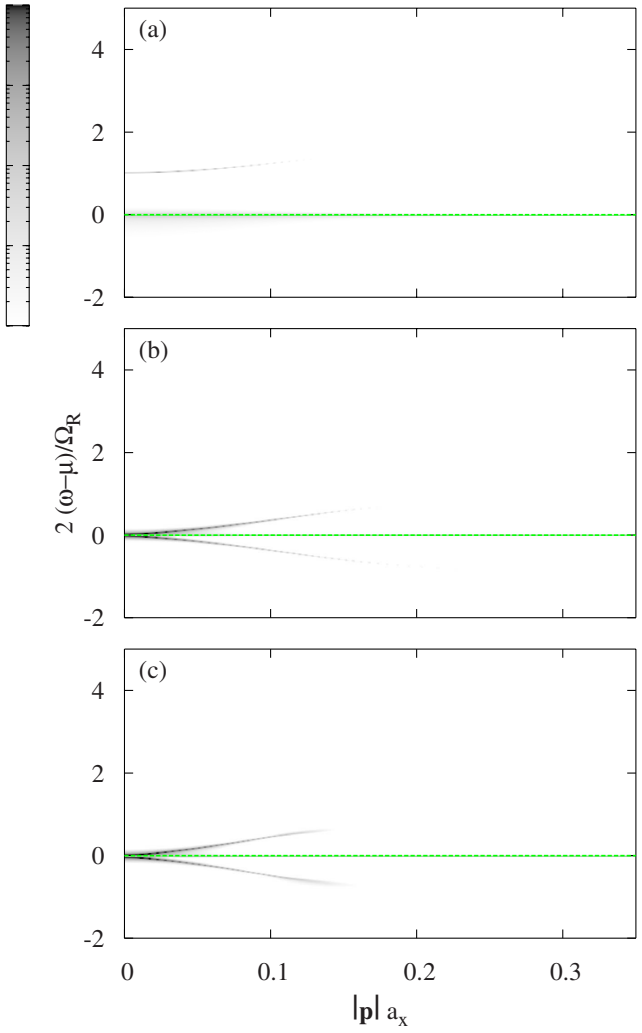

FIG. 8. (Color online) Contour plot of the incoherent PL $P(\omega,\mathbf{p})$ as a function of the dimensionless momentum $|\mathbf{p}|a_x$ and rescaled energy $2(\omega-\mu)/\Omega_R$, for detuning $\omega_0-E_x=-0.94$ meV, $\Omega_R=26$ meV, $k_BT=20$ K, and $m_{\rm ph}\Omega_R a_x^2/2=0.01$: (a) noncondensed ($\rho\simeq 0$, $E_x-\mu\simeq 27$ meV), (b) condensed ($\rho\simeq 7.8\times 10^{-3}$, $E_x-\mu\simeq 11$ meV), and (c) condensed ($\rho\simeq 6.7\times 10^{-2}$, $E_x-\mu\simeq 7$ meV).

normal modes requires a relatively large condensate density. Due to instrumental broadening, the presence of emission from this large condensate density might obscure emission from the normal modes, so they may only be weakly visible, as shown in Fig. 8. As discussed below, RRS may provide a means of escape from this problem.

B. Lower polariton blueshift

Before discussing the RRS response, let us briefly discuss a point mentioned above—the calculation of the LP blueshift as a function of density, making use of the full density of states, and our model of saturation effects (1). This can be observed in PL experiments by the change of blueshift as a function of intensity of the nonresonant pumping.

In the noncondensed regime, the blueshift of the LP in our model is a consequence of the saturation of the (disordered)

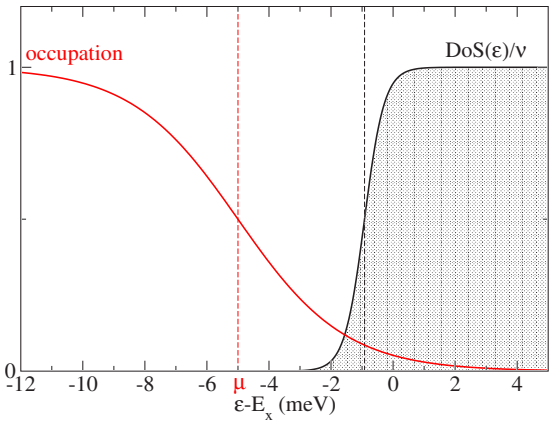

FIG. 9. (Color online) Normalized density of states $\mathrm{DOS}(\varepsilon)/\nu$ and thermal occupation factor [red (gray) line starting at top left] for $E_x-\mu=5$ meV and $k_BT=20$ K.

energy levels. Following the narrow bandwidth limit described in Eq. (19), this saturation blueshift can be found if one has an expression for the chemical potential at a given temperature and density. In the low-density limit, the expression for density ρ as a function of μ [Eq. (12) with $\psi=0$] can be inverted in terms of elementary functions. As illustrated in Fig. 9, in the low-density limit, the chemical potential is far below the band edge. Thus, there are two significant contributions to density: one from low energies, in the tail of the DOS, but at large occupation, and one from high energies, in the tail of the occupation, but at large DOS, thus

$$\rho \simeq \int_{-\infty}^{\mu} \frac{d\varepsilon}{\mathcal{R}y_x} e^{-2|\varepsilon|/W_\rho} + \int_0^{\infty} \frac{d\varepsilon}{\mathcal{R}y_x} e^{-(\varepsilon-\mu)/k_BT}. \tag{20}$$

Here, $W_\rho/2=0.32$ meV is the energy which characterizes the exponential decay of DOS in the tail of the Lifshitz states—this coefficient is extracted by an exponential fit to our numerical DOS. At a temperature of $k_BT=20$ K$=1.72$ meV, the dominant contribution to the density is given by the second integral and the chemical potential increases logarithmically with the density:

$$\rho \simeq \frac{k_BT}{\mathcal{R}y_x} e^{\mu/k_BT}. \tag{21}$$

From this expression, and from the coupled oscillator expressions of the LP Eq. (19), we can explicitly derive the reduced Rabi splitting due to saturation effects,

$$\bar{\Omega}_R \simeq \Omega_R \left(1 - 2e^{-\varepsilon^*/k_BT} \frac{\mathcal{R}y_x}{k_BT}\rho\right)^{1/2},$$

and the LP blueshift, which is thus linear in this low-density regime,

$$\delta E_{\rm LP} \equiv E_{\rm LP}(\rho) - E_{\rm LP}(0) \sim \Omega_R n \frac{1}{m_x k_BT}, \tag{22}$$

where we have reintroduced here the density n per unit volume. Remaining at small densities, but now considering the low temperature limit, $W_\rho/2 > k_BT$, then the dominant term in Eq. (20) is the first, and so Eq. (22) should be modified by

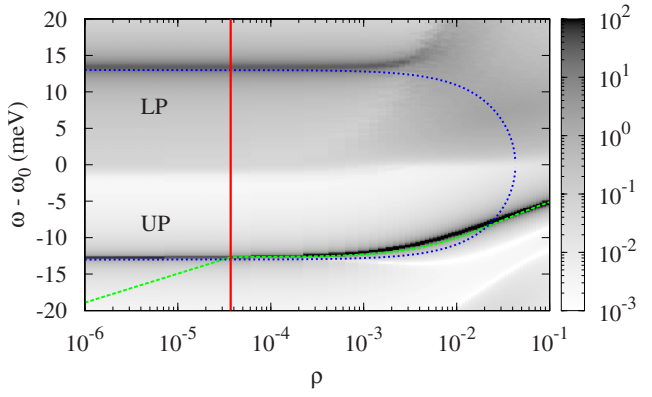

FIG. 10. (Color online) Contour plot of the spectral weight $W(\omega,0)$ for $\mathbf{p}=0$ as a function of the dimensionless density ρ and the rescaled energy $\omega-\omega_0$, for zero detuning ($\omega_0-E_x=-0.94$ meV) and $k_BT=20$ K ($2k_BT/\Omega_R=0.13$). The rescaled chemical potential ($\mu-\omega_0$) [green (light gray) dashed], the noncondensed lower and upper polariton modes from the two coupled oscillator model [blue (dark gray) dotted], and the critical density for condensation $\rho_c\simeq 3.7\times10^{-5}$ [vertical solid red (dark gray) line] are shown for comparison.

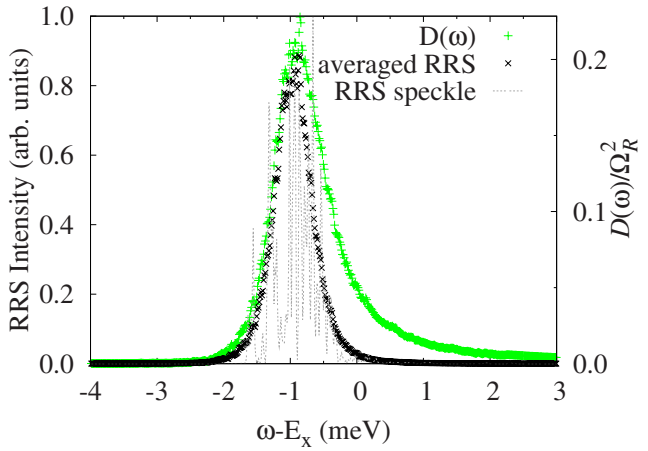

FIG. 11. (Color online) Excitonic speckle pattern $|K^{(1o)}_{\mathbf{p},\mathbf{q}}(\omega_h)|^2|_{i\omega_h=-\omega-i\eta}$ for a single disorder realization (gray dotted line) and its disorder average (black cross symbols) versus energy for $|\mathbf{p}|=|\mathbf{q}|=36°$ and a 90° azimuthal angle, $\mathbf{p}=(0,6.3\times10^4)$ cm^{-1} and $\mathbf{q}=(6.3\times10^4,0)$ cm^{-1}. For comparison, we also plot the excitonic optical density [green (light gray) plus symbols].

replacing the thermal length $(m_xk_BT)^{-1}$ by a characteristic disorder length $(m_xW_\rho)^{-1}$.

It is instructive to compare this result with that for a clean system; in this case, blueshift of the LP has been attributed either due to Coulomb interaction[53] or to saturation effects[54] (where the expression given here is valid only in the dilute limit):

$$\delta E^0_{\mathrm{Coul}}\sim \mathcal{R}y_x n a_x^2,$$

$$\delta E^0_{\mathrm{sat}}\sim \Omega_R n a_x^2.$$

Because the excitonic Rydberg $\mathcal{R}y_x$ can be of the same order of magnitude as the Rabi splitting Ω_R, in a clean system the two shifts can be expected to be of the same order of magnitude. Considering just saturation effects, the difference between clean and dirty systems is that, at low temperature, in a clean system blueshift depends on exciton number per square Bohr radius, while in a disordered system, the relevant length is that characteristic of the disorder potential, which is, in general, larger than the Bohr radius. Finally, we wish to observe that there is a distinction between Coulomb and saturation effects: Coulomb interactions result in a blueshift of both the LP and UP, while saturation leads to a blueshift of the LP and a redshift of the UP, i.e., a collapse of the Rabi splitting. Thus, these effects can be experimentally distinguished and their relative magnitudes determined.

In the condensed regime, the equivalent of the LP is the Goldstone linear mode, which by definition starts at the chemical potential. Thus, the observed blueshift is a direct observation of chemical potential vs density. Figure 10 shows the variation of the spectral weight at zero momentum as a function of density, from which the energy of the zero momentum LP and UP modes can be extracted. Also shown, for comparison, is the chemical potential vs density (dashed green line). The locking of the LP mode to the chemical potential beyond the critical density (red solid line) is clearly visible, and the behavior of the LP mode vs density allows the extraction of density from an experimental measurement of LP blueshift.

C. Resonant Rayleigh scattering

As described in Refs. 35 and 36, the RRS intensity describes the probability to inject a photon into the cavity with momentum $\mathbf{p}$ and detect a coherent photon at $\mathbf{q}$ with $\mathbf{p}\neq\mathbf{q}$. The intensity of such a signal may be written as

$$I_{\mathbf{pq}}(\omega)=|\mathcal{G}^{11}_{\mathbf{pq}}|^2|_{i\omega_h=-\omega-i\eta}. \tag{23}$$

Since this involves the off-diagonal momentum space components of the Green's function, it is necessary to include the off-diagonal momentum components of the inverse Green's function Eq. (16). However, as discussed in Sec. III, we will consider only a single polariton scattering and again neglect multiple polariton scattering (but include all orders of exciton-disorder scattering). Such an approximation is reasonable for the same reasons discussed at the start of Sec. III.

In the following, we propose using the RRS signal to probe the excitation spectrum in the presence of a polariton condensate. It is, therefore, necessary to be able to separate the RRS signal from the strong photoluminescence that would arise from the equilibrium state with large polariton density. Further, since a condensed polariton system may have a strong nonlinear response to an applied probe (i.e., stimulated scattering if the probe significantly affects the population of polariton modes), it is necessary to use a weak RRS probe. Fortunately, the coherent nature of RRS allows exactly this: one can detect a weak RRS signal by phase sensitive measurement, as is discussed in detail in the Appendix. Hence, the limit on intensity of the probe is provided by the sensitivity of the charge coupled device camera and

not by the incoherent photoluminescence background. This, therefore, allows a probe sufficiently weak that only the linear RRS response is seen and nonlinear effects are avoided.

When noncondensed, the single polariton scattering expansion of the photon Green's function in the off-diagonal terms gives

$$I_{\mathbf{pq}}(\omega_h) \simeq \frac{1}{|K^{(1)}_{\mathbf{pp}}(\omega_h)|^2} |K^{(1)o}_{\mathbf{pq}}(\omega_h)|^2 \frac{1}{|K^{(1)}_{\mathbf{qq}}(\omega_h)|^2}. \quad (24)$$

The factors $|K^{(1)}_{\mathbf{qq}}(\omega_h)|^{-2}$ appearing here can be interpreted as a filter, allowing a response only when the outgoing (or, equivalently, incoming for $\mathbf{q} \to \mathbf{p}$) momentum has an energy close to the polariton mode at the given energy. This means that $|\mathbf{p}| \simeq |\mathbf{q}|$ and so is responsible for the ring-shaped RRS signal observed in experiments.[37,38] In contrast, the term $|K^{(1o)}_{\mathbf{p,q}}(\omega_h)|^2$ describes scattering between momentum states via polariton-exciton-polariton scattering. This term has a large variation from disorder realization to disorder realization, and is the reason for the speckle seen in RRS experiments. This speckle and the disorder averaged RRS intensity are shown for comparison in Fig. 11. As the precise speckle pattern depends on the precise disorder realization, the most we can reasonably do is to describe the statistical properties of this speckle; thus, the disorder averaged RRS signal shown in Fig. 1 would, in experiment, represent the envelope of the RRS speckle pattern.

When condensed, the expression for the RRS intensity becomes more complicated, but can still be written in the form of a filter and a scattering part:

$$I_{\mathbf{pq}}(\omega) = \simeq F_{\mathbf{p}} S_{\mathbf{pq}} F_{\mathbf{q}}, \quad (25)$$

where the filter and scattering terms are respectively

$$F_{\mathbf{p}} = \left| |K^{(1)}_{\mathbf{pp}}|^2 - (K^{(2)}_{\mathbf{pp}})^2 \right|^{-2},$$

$$S_{\mathbf{pq}} = |K^{(1)o}_{\mathbf{pq}} K^{(1)*}_{\mathbf{pp}} K^{(1)*}_{\mathbf{qq}} + K^{(1)o*}_{\mathbf{qp}} K^{(2)}_{\mathbf{pp}} K^{(2)}_{\mathbf{qq}} - K^{(2)o}_{\mathbf{pq}} (K^{(2)}_{\mathbf{pp}} K^{(1)*}_{\mathbf{qq}} + K^{(1)*}_{\mathbf{pp}} K^{(2)}_{\mathbf{qq}})|^2. \quad (26)$$

As in the noncondensed case, the filter function $F_{\mathbf{p}}$ restricts the allowed incoming and outgoing momenta to those for which the normal modes have the injected energy. However, as discussed earlier, in the presence of a condensate, the normal modes supported are no longer the LP and UP, but are, instead, the new Bogoliubov-like quasimodes.

The decay of spectral weight associated with modes far below the chemical potential, as discussed in Sec. III A, still applies (this can clearly be seen in Figs. 1, 6, and 8). However, since the energy of the RRS signal is controlled by the energy of the incident photon, it is possible to study modes far above the chemical potential, which would have negligible equilibrium occupation and, thus, negligible weight in the PL signal. Both for this reason and because of the ability to discriminate between the coherent RRS signal and incoherent photoluminescence, RRS provides a very powerful tool to study the interesting properties of condensed polariton systems.

IV. CONCLUSIONS

In this paper, we have analyzed and compared different optical responses of a condensate of microcavity polaritons. One of the conclusions of this work is that, compared to photoluminescence studies, the energy- and momentum-resolved resonant Rayleigh scattering spectra provide many advantages in probing a condensed phase and in studying the associated coherent excitation spectrum. In particular, resonant Rayleigh scattering, by collecting the signal at a different angle from that at which the system is probed, allows one to look directly at characteristic features of the condensed phase excitation spectrum. Such features, like the Goldstone modes both above and below the chemical potential, are weak in photoluminescence emission and are likely to be masked by the strong emission from the condensate in the lowest momentum state. In contrast, Rayleigh scattering, being coherent with the probe, can be distinguished from condensate emission.

One may ask why the accurate description of excitonic disorder considered in this paper is necessary, when the microcavity photon introduces a long length scale that averages over disorder. One might also compare this system with other excitonic systems, such as double quantum wells,[55] where the high density of dipole-dipole interacting excitons quickly screens the disorder.[56,57] The answer to this question is that the large ratio of exciton to photon mass means, first, that exciton density required for condensation in microcavities is far less than in double quantum wells, and second, that those exciton states involved in forming the thermally occupied polariton modes are strongly localized exciton states (i.e., influenced by disorder beyond Born approximation). One of the consequences of an accurate treatment of disorder in microcavities is that the blueshift of the lower polaritons due to saturation effects depends on a length scale characteristic of disorder and temperature, which can be much larger than the Bohr radius, this length playing an equivalent role in the clean system. This effect can be important in determining the polariton densities from the measured blueshift in current experiments.

An important consequence of disorder is that the exciton-light coupling strength is characterized by a full distribution. In the noncondensed phase, the optical density alone determines the photoluminescence response, while for resonant Rayleigh scattering, the averaged fourth power of the oscillator strength is required. However, in the condensed phase, one has to consider the entire distribution for each exciton energy. For energies close to and above the band edge, there is always a nonvanishing probability of an arbitrarily small oscillator strength. For this reason, in contrast to examples like BCS superconductivity, one can show that the quasiparticle spectrum does not have a hard gap.

In conclusion, we have considered how an accurate treatment of disorder on the single-particle excitonic level, when elevated to the many-body problem of interacting microcavity polaritons, leads to a variety of interesting features in various optical responses and probes of the condensed phase.

ACKNOWLEDGMENTS

We are grateful to Roland Zimmermann, Wolfgang Lang-

bein, and Ben Simons for suggestions and useful discussions. F.M.M. and M.H.S. would like to acknowledge financial support from EPSRC. J.K. would like to acknowledge financial support from the Lindemann Trust. This work is supported by the EU Network "Photon mediated phenomena in semiconductor nanostructures" HPRN-CT-2002-00298.

APPENDIX: PHASE SENSITIVE DETECTION OF RESONANT RAYLEIGH SIGNAL

In this appendix, we show how the coherent nature of the resonant Rayleigh signal allows a weak coherent probe to be detected in the presence of strong incoherent photoluminescence. The Rayleigh scattering probe is a perturbation, $\hat{H}=\hat{H}_0+\hat{V}$, which in the rotating wave approximation may be written as

$$\hat{V}=A_0(\hat{\psi}_{\mathbf{p}}^{\dagger}e^{i\Omega t}+\hat{\psi}_{\mathbf{p}}e^{-i\Omega t}). \tag{A1}$$

This describes a probe at wave vector $\mathbf{p}$, frequency Ω, of strength A_0. The RRS signal is the coherent scattering of this probe to other wave vectors. To isolate the part of the emission that is coherent with the probe, one may use a homodyne measurement, interfering the emission with part of the probe signal. This corresponds to measuring the spectrally resolved emission intensity:

$$P(\omega,\mathbf{q})=\int dt e^{i\omega t}P(t,\mathbf{q}), \tag{A2}$$

where

$$P(t,\mathbf{q})=\sum_n e^{\beta(F-E_n)}\langle n|[\hat{\psi}_{\mathbf{q}}^{\dagger}(t)+A_1e^{-i(\Omega t+\phi)}][\hat{\psi}_{\mathbf{q}}(0)+A_1e^{i\phi}]|n\rangle,$$

and where A_1 is the strength of the homodyne mixing and ϕ is a phase delay introduced between the probe and the homodyne signal. The states $|n\rangle$ are the eigenstates of the system without the probe, given by $\hat{H}_0|n\rangle=E_n|n\rangle$; F is the free energy, for normalization.

The principle of phase sensitive detection is to vary the phase delay and to extract the part of $P(\omega,\mathbf{q})$ that depends on this phase delay. Since the background PL does not depend on the phase delay, this allows one to separate a small but phase-dependent signal from a strong but phase-independent background.

The part of the signal that depends on phase is

$$P_{\phi}(t,\mathbf{q})=A_1\sum_n e^{\beta(F-E_n)}[\langle n|\hat{\psi}_{\mathbf{q}}^{\dagger}(t)|n\rangle e^{i\phi}+\langle n|\hat{\psi}_{\mathbf{q}}(0)|n\rangle e^{-i(\phi+\Omega t)}]. \tag{A3}$$

Standard first order time-dependent perturbation theory, using the perturbation in Eq. (A1), yields

$$\langle n|\hat{\psi}_{\mathbf{q}}^{\dagger}(t)|n\rangle=A_0\sum_m\left[\frac{\langle n|\hat{\psi}_{\mathbf{q}}^{\dagger}|m\rangle\langle m|\hat{\psi}_{\mathbf{p}}|n\rangle}{E_n-E_m-\Omega-i\eta}-\frac{\langle n|\hat{\psi}_{\mathbf{p}}|m\rangle\langle m|\hat{\psi}_{\mathbf{q}}^{\dagger}|n\rangle}{E_m-E_n-\Omega-i\eta}\right]e^{-i\Omega t}+[\ldots]e^{i\Omega t}. \tag{A4}$$

The term written $[\ldots]$ is similar to the first term, but with $\Omega\mapsto-\Omega$ and $\psi_{\mathbf{p}}\leftrightarrow\psi_{\mathbf{p}}^{\dagger}$. Inserting this signal into Eq. (A3) and then into Eq. (A2), it can be seen that such a term gives a signal at frequency $\omega=-\Omega$, and so can be clearly separated and ignored. Inserting the first term into Eq. (A3), one can write

$$\sum_n e^{\beta(F-E_n)}\langle n|\hat{\psi}_{\mathbf{q}}^{\dagger}(t)|n\rangle=\sum_{n,m}e^{\beta(F-E_n)}[1-e^{\beta(E_n-E_m)}]\times\frac{\langle n|\hat{\psi}_{\mathbf{q}}^{\dagger}|m\rangle\langle m|\hat{\psi}_{\mathbf{p}}|n\rangle}{E_n-E_m-\Omega-i\eta}, \tag{A5}$$

which is the definition of the retarded Green's function,[48] $G_{R,\mathbf{pq}}^{11}(\Omega)=\mathcal{G}_{\mathbf{pq}}^{11}|_{i\omega_h=-\Omega-i\eta}$. By repeating the same analysis for the second term in Eq. (A3), one can then write

$$P_{\phi}(t,\mathbf{q})=2A_1A_0|G_{R,\mathbf{pq}}^{11}(\Omega)|\cos(\phi+\phi_0)e^{-i\Omega t}, \tag{A6}$$

where ϕ_0 is the phase of the retarded Green's function. Hence, the phase-dependent part of the luminescence is given by the off-diagonal in momentum space part of the retarded Green's function, i.e., the RRS signal.

*Present address: Rudolf Peierls Centre for Theoretical Physics, 1 Keble Road, Oxford OX1 3NP, UK.
†Present address: Cavendish Laboratory, University of Cambridge, Madingley Road, Cambridge CB3 0HE, UK.

[1] L. V. Keldysh and Yu. V. Kopaev, Fiz. Tverd. Tela (Leningrad) **6**, 2791 (1964); [Sov. Phys. Solid State **6**, 2219 (1965)].
[2] J. J. Hopfield, Phys. Rev. **112**, 1555 (1958).
[3] C. Weisbuch, M. Nishioka, A. Ishikawa, and Y. Arakawa, Phys. Rev. Lett. **69**, 3314 (1992).
[4] Le Si Dang, D. Heger, R. André, F. Boeuf, and R. Romestain, Phys. Rev. Lett. **81**, 3920 (1998).
[5] P. Senellart and J. Bloch, Phys. Rev. Lett. **82**, 1233 (1999).
[6] Y. Yamamoto, Nature (London) **405**, 629 (2000).
[7] P. G. Savvidis, J. J. Baumberg, R. M. Stevenson, M. S. Skolnick, D. M. Whittaker, and J. S. Roberts, Phys. Rev. Lett. **84**, 1547 (2000).
[8] M. Saba, C. Ciuti, J. Bloch, V. Thierry-Mieg, R. André, Le Si Dang, S. Kundermann, A. Mura, G. Bongiovanni, J. L. Staehli, and B. Deveaud, Nature (London) **414**, 731 (2001).
[9] H. Deng, G. Weihs, C. Santori, J. Bloch, and Y. Yamamoto, Science **298**, 199 (2002); H. Deng, G. Weihs, D. Snoke, J. Bloch, and Y. Yamamoto, Proc. Natl. Acad. Sci. U.S.A. **100**, 15318 (2003).
[10] G. Weihs, H. Deng, D. Snoke, and Y. Yamamoto, Phys. Status Solidi A **201**, 625 (2004).
[11] M. Richard, J. Kasprzak, R. Romestain, R. André, and L. S. Dang, Phys. Rev. Lett. **94**, 187401 (2005).
[12] M. Richard, J. Kasprzak, R. André, R. Romestain, L. S. Dang, G.

Malpuech, and A. Kavokin, Phys. Rev. B **72**, 201301(R) (2005).
[13] H. Deng, D. Press, S. Gotzinger, G. S. Solomon, R. Hey, K. H. Ploog, and Y. Yamamoto, Phys. Rev. Lett. **97**, 146402 (2006).
[14] J. Kasprzak, M. Richard, S. Kundermann, A. Baas, P. Jeanbrun, J. Keeling, F. M. Marchetti, M. H. Szymanska, R. Andre, J. L. Staehli, V. Savona, P. B. Littlewood, B. Devaud, and Le Si Dang, Nature (London) **443**, 409 (2006).
[15] F. Tassone, C. Piermarocchi, V. Savona, A. Quattropani, and P. Schwendimann, Phys. Rev. B **56**, 7554 (1997); F. Tassone and Y. Yamamoto, *ibid.* **59**, 10830 (1999).
[16] A. I. Tartakovskii, M. Emam-Ismail, R. M. Stevenson, M. S. Skolnick, V. N. Astratov, D. M. Whittaker, J. J. Baumberg, and J. S. Roberts, Phys. Rev. B **62**, R2283 (2000).
[17] P. R. Eastham and P. B. Littlewood, Solid State Commun. **116**, 357 (2000); Phys. Rev. B **64**, 235101 (2001).
[18] M. H. Szymanska and P. B. Littlewood, Solid State Commun. **124**, 103 (2002); M. H. Szymanska, P. B. Littlewood, and B. D. Simons, Phys. Rev. A **68**, 013818 (2003).
[19] A. Kavokin and G. Malpuech, *Cavity Polaritons*, Thin Films and Nanostructures Vol. 32 (Elsevier, New York, 2003).
[20] F. P. Laussy, G. Malpuech, A. Kavokin, and P. Bigenwald, Phys. Rev. Lett. **93**, 016402 (2004); A. Kavokin, G. Malpuech, and F. P. Laussy, Phys. Lett. A **306**, 187 (2003).
[21] J. Keeling, P. R. Eastham, M. H. Szymanska, and P. B. Littlewood, Phys. Rev. Lett. **93**, 226403 (2004); Phys. Rev. B **72**, 115320 (2005).
[22] F. M. Marchetti, B. D. Simons, and P. B. Littlewood, Phys. Rev. B **70**, 155327 (2004); F. M. Marchetti, M. H. Szymanska, P. R. Eastham, B. D. Simons, and P. B. Littlewood, Solid State Commun. **134**, 111 (2005).
[23] T. D. Doan, H. T. Cao, D. B. Tran Thoai, and H. Haug, Phys. Rev. B **72**, 085301 (2005).
[24] I. Shelykh, F. P. Laussy, A. V. Kavokin, and G. Malpuech, arXiv:cond-mat/0503402 (unpublished).
[25] F. M. Marchetti, J. Keeling, M. H. Szymanska, and P. B. Littlewood, Phys. Rev. Lett. **96**, 066405 (2006).
[26] M. H. Szymańska, J. Keeling, and P. B. Littlewood, Phys. Rev. Lett. **96**, 230602 (2006).
[27] D. Porras and C. Tejedor, Phys. Rev. B **67**, 161310(R) (2003).
[28] D. Sarchi and V. Savona, in *Physics of Semiconductors: 28th International Conference on the Physics of Semiconductors—ICPS 2006*, AIP Conf. Proc No. 893 (AIP, New York, 2007), p. 401.
[29] P. Schwendimann and A. Quattropani, Phys. Rev. B **74**, 045324 (2006).
[30] R. Zimmermann, F. Grosse, and E. Runge, Pure Appl. Chem. **69**, 1179 (1997); R. Zimmermann and E. Runge, Phys. Status Solidi A **164**, 511 (1997).
[31] E. Runge and R. Zimmermann, in *Advances in Solid State Physics*, edited by B. Kramer (Vieweg, Braunschweig, 1998) Vol. 38; Phys. Status Solidi B **221**, 269 (2000).
[32] E. Runge, *Excitons in Semiconductors Nanostructures*, Solid State Physics Vol. 57 (Academic, Amsterdam, 2002).
[33] D. M. Whittaker, Phys. Rev. Lett. **80**, 4791 (1998).
[34] P. Borri, W. Langbein, U. Woggon, J. R. Jensen, and J. M. Hvam, Phys. Rev. B **63**, 035307 (2000).
[35] D. M. Whittaker, Phys. Rev. B **61**, R2433 (2000).
[36] A. V. Shchegrov, J. Bloch, D. Birkedal, and J. Shah, Phys. Rev. Lett. **84**, 3478 (2000).
[37] T. Freixanet, B. Sermage, J. Bloch, J. Y. Marzin, and R. Planel, Phys. Rev. B **60**, R8509 (1999).
[38] W. Langbein and J. M. Hvam, Phys. Rev. Lett. **88**, 047401 (2002).
[39] I. Carusotto and C. Ciuti, Phys. Rev. Lett. **93**, 166401 (2004); C. Ciuti and I. Carusotto, Phys. Status Solidi B **242**, 2224 (2005).
[40] J. Keeling, F. M. Marchetti, M. H. Szymańska, and P. B. Littlewood, Semicond. Sci. Technol. **22**, R1 (2007).
[41] S. D. Baranovskii and A. L. Éfros, Fiz. Tekh. Poluprovodn. (S.-Peterburg) **12**, 2233 (1978) [Sov. Phys. Semicond. **12**, 1328 (1979)].
[42] N. N. Ablyazov, M. É. Raikh, and A. L. Éfros, Fiz. Tverd. Tela (Leningrad) **25**, 353 (1983) [Sov. Phys. Solid State **25**, 199 (1983)].
[43] M. Litinskaia, G. C. La Rocca, and V. M. Agranovich, Phys. Rev. B **64**, 165316 (2001).
[44] R. Zimmermann, E. Runge, and V. Savona, in *Quantum Coherence, Correlation and Decoherence in Semiconductor Nanostructures*, edited by T. Takagahar (Elsevier Science, New York, 2003).
[45] I. M. Lifshitz, Adv. Phys. **13**, 483 (1964); J. Zittartz and J. S. Langer, Phys. Rev. **148**, 741 (1966); B. I. Halperin and M. Lax, *ibid.* **148**, 722 (1966).
[46] M. C. Payne, M. P. Teter, D. C. Allan, T. A. Arias, and J. D. Joanopoulos, Rev. Mod. Phys. **64**, 1045 (1992).
[47] M. Gurioli, F. Bogani, L. Cavigli, H. Gibbs, G. Khitrova, and D. S. Wiersma, Phys. Rev. Lett. **94**, 183901 (2005).
[48] A. A. Abrikosov, L. P. Gor'kov and I. E. Dzyaloshinski, *Methods of Quantum Field Theory in Statistical Physics* (Dover, New York, 1975).
[49] R. Houdré, R. P. Stanley, and M. Ilegems, Phys. Rev. A **53**, 2711 (1996).
[50] A. V. Mintsev, L. V. Butov, C. Ell, S. Mosor, G. Khitrova, and H. M. Gibbs, Pis'ma Zh. Eksp. Teor. Fiz. **76**, 742 (2002); [JETP Lett. **76**, 637 (2002)].
[51] L. P. Pitaevskii and S. Stringari, *Bose Einstein Condensation* (Clarendon, Oxford, 2003).
[52] J. Kasprzak, R. Andre, L. S. Dang, I. A. Shelykh, A. V. Kavokin, Y. G. Rubo, K. V. Kavokin, and G. Malpuech, Phys. Rev. B **75**, 045326 (2007).
[53] G. Rochat, C. Ciuti, V. Savona, C. Piermarocchi, A. Quattropani, and P. Schwendimann, Phys. Rev. B **61**, 13856 (2000).
[54] C. Ciuti, P. Schwendimann, B. Deveaud, and A. Quattropani, Phys. Rev. B **62**, R4825 (2000).
[55] L. V. Butov, J. Phys.: Condens. Matter **16**, R1577 (2004).
[56] A. L. Ivanov, Europhys. Lett. **59**, 586 (2002).
[57] R. Zimmermann, Solid State Commun. **134**, 43 (2005).